Prediction of plateau and peak of pressure in a compression ramp flow with large separation

Article *in* Physics of Fluids · October 2020

DOI: 10.1063/5.0024101

4 authors, including:

Wenfeng Zhou
Peking University
16 PUBLICATIONS **38** CITATIONS

SEE PROFILE

Prediction of plateau and peak of pressure in a compression ramp flow with large separation

Cite as: Phys. Fluids **32**, 101702 (2020); https://doi.org/10.1063/5.0024101
Submitted: 04 August 2020 . Accepted: 12 September 2020 . Published Online: 02 October 2020

Yan-Chao Hu (胡延超), Wen-Feng Zhou (周文丰), Yan-Guang Yang (杨彦广), and Zhi-Gong Tang (唐志共)

Physics of Fluids LETTER scitation.org/journal/phf

Prediction of plateau and peak of pressure in a compression ramp flow with large separation

Cite as: Phys. Fluids 32, 101702 (2020); doi: 10.1063/5.0024101
Submitted: 4 August 2020 • Accepted: 12 September 2020 •
Published Online: 2 October 2020

Yan-Chao Hu (胡延超),[1] Wen-Feng Zhou (周文丰),[1,2] Yan-Guang Yang (杨彦广),[3,a)] and Zhi-Gong Tang (唐志共)[3,a)]

AFFILIATIONS

[1]Hypervelocity Aerodynamics Institute, China Aerodynamics Research and Development Centre, Mianyang 621000, China
[2]State Key Laboratory for Turbulence and Complex Systems, College of Engineering, Peking University, Beijing 100871, China
[3]China Aerodynamics Research and Development Centre, Mianyang 621000, China

[a)]**Authors to whom correspondence should be addressed:** yangyanguang@cardc.cn and tangzhigong@126.com

ABSTRACT

Based on the Helmholtz–Rayleigh minimal dissipation theorem, a theoretical model is proposed to predict both the plateau and peak of pressure in a compression ramp flow with large separation (CRFLS). Since the total dissipation of CRFLS is mainly contributed by the shock waves, the steady flow pattern can be determined by minimizing the shock dissipation among all the possible configurations. The predictions agree well with both experimental data and numerical simulations, covering a wide range of free-stream Mach number and ramp angle. This method could be applied to other flow systems where the dissipation is dominated by shock waves.

The compression ramp flow (CRF) is a canonical system of shock wave/boundary layer interactions.[1] The pressure p distribution of compression ramp flow with large separation (CRFLS) has been investigated widely.[2–10] As shown in Fig. 1(a), a key feature of the distribution is the emergence of a pressure plateau p_{pla} in the recirculation region. The free-interaction theory (FIT) established by Chapman[2] argues that the supersonic separation is a local self-induced free-interaction process between the incoming boundary layer and the outer inviscid stream, supplying a plateau pressure for laminar interaction,[11]

$$\frac{p_{pla}-p_i}{p_i}=1.5\frac{\gamma M_0^2 C_{f,i}^{1/2}}{\sqrt{2}\left(M_0^2-1\right)^{1/4}}, \tag{1}$$

where M_0 is the free-stream Mach number. $C_{f,i}$ and p_i are the skin-friction coefficient and wall pressure at the interaction origin I, respectively. γ is the ratio of specific heats. Equation (1) has been widely confirmed by experiments and simulations,[1,2,11] suggesting that for a given M_0, p_{pla} depends only on the flow conditions ($C_{f,i}$ and p_i) at I rather than the downstream conditions.

Using an asymptotic expansion technique, Stewartson and Williams[5] and Neiland[6] simultaneously formulated the triple-deck theory describing the interaction process more elaborately. Numerical solutions of this theory[8–10] have shown that the pressure plateau arises for $\alpha^* \geq 2.5$ (criterion of large separation) and fully develops for $\alpha^* \geq 3.5$. α^* is a scaled ramp angle defined[7] as $\alpha^* = \frac{\alpha Re^{1/4}}{C^{1/4}\lambda^{1/2}(M_0^2-1)^{1/4}}$, where α is the geometric ramp angle. Re is the characteristic Reynolds number based on the flat plate length l and the free-stream conditions. C is the Chapman–Rubesin parameter and $\lambda = 0.332$ is the shear constant of a Blasius boundary layer. In terms of this theory,[12,13] the separation process from the interaction origin point I to the separation point S is $O(lRe^{-3/8})$, the plateau region is $O(l)$, and the reattachment process is $O(lRe^{-1/2})$, implying that the streamwise extents of the separation and reattachment processes can be negligible compared with the plateau region for a sufficient large Re. Therefore, the separation bubble has an approximately triangular shape.[14] It forms a virtual ramp between the flat

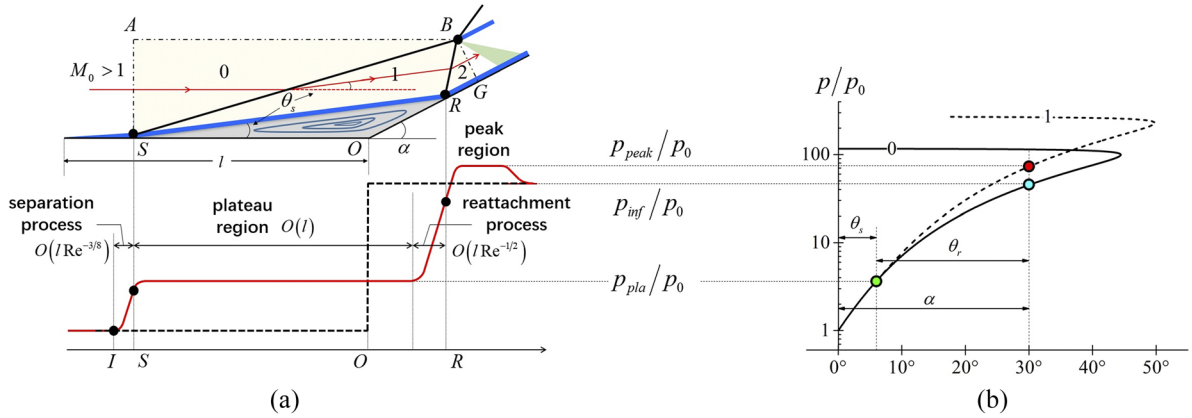

FIG. 1. (a) Upper panel: CRFLS configuration and lower panel: distributions of wall pressure p_w; red solid line—large separation case and black dashed line—inviscid case. (b) Shock polars ($M_0 = 10$, $\alpha = 30°$, and $\theta_s = 6°$).

plate and the ramp, deflecting the outer-stream twice with angle θ_s and $\theta_r = \alpha - \theta_s$. The λ-shock pattern induced by the two deflections has been classified as type VI by Edney,[15] as shown in Fig. 1(a). For hypersonic cases ($M_0 > 5$), a distinct pressure peak p_{peak} also appears behind reattachment on which some semi-empirical expressions have been established.[16] Shock polars in Fig. 1(b) show that both p_{pla} and p_{peak} are determined by θ_s, indicating the crucial role of θ_s.[17]

Herein, we use the minimal viscous dissipation (MVD) theorem to predict p_{pla} and p_{peak}. In terms of the CRFLS configuration, we can obtain θ_s by minimizing the total dissipation of the shock waves. Then, both p_{pla} and p_{peak} are predictable. Two-dimensional (2D) CRF simulations for different M_0 and α are also performed for validation. Predictions of p_{pla} and p_{peak} agree well with both experiments and simulations.

For steady flows, the process of the kinetic energy dissipated by viscosity is governed by the kinetic energy equation,

$$\rho \boldsymbol{u} \cdot \nabla\left(\frac{1}{2}|\boldsymbol{u}|^2\right) = \rho \boldsymbol{f} \cdot \boldsymbol{u} + p\vartheta + \nabla \cdot (\boldsymbol{T} \cdot \boldsymbol{u}) - \phi, \tag{2}$$

where ρ, $\boldsymbol{u}$, $\boldsymbol{f}$, and p are the density, velocity, body force, and pressure, respectively. $\vartheta = \nabla \cdot \boldsymbol{u}$, $\boldsymbol{D} = \left[\nabla \boldsymbol{u} + (\nabla \boldsymbol{u})^T\right]/2$, and $\mathbf{T} = (-p + \eta\vartheta)\mathbf{I} + 2\mu\mathbf{D}$ are the velocity divergence, strain-rate tensor, and stress tensor, respectively. η and μ are the dilatation viscosity and shear viscosity of the flow, respectively. ϕ is the viscous dissipation,

$$\phi = \eta\vartheta^2 + 2\,\mu \boldsymbol{D} : \boldsymbol{D}. \tag{3}$$

The Helmholtz–Rayleigh MVD theorem[18–20] has demonstrated that an incompressible viscous flow should have MVD if acceleration $\mathbf{a}$ can be derived by a potential ζ ($\mathbf{a} = \nabla\zeta$), i.e., the total dissipation $\Phi = \int_V \phi \mathrm{d}V$ in a control volume V has the minimal value with no dissipation on V's boundaries. Ho *et al.*[21–23] have generalized this MVD theorem to compressible flows satisfying that (i) the flow acceleration can be derived by a potential, (ii) the body force can be derived by a potential, and (iii) the flow is barotropic. According to vector operation, a flow passing through a shock wave satisfies these three conditions, implying that a steady shock configuration should satisfy MVD (see proof in Part 1 of the supplementary material).

In a CRFLS, an appropriate control volume V shown in Fig. 1(a) is bounded by AB, BG, GO, OS, and SA, enclosing the interaction region, where B and O are the triple point and ramp apex, respectively. The flow structures in V consist of shock waves SB and RB, shear layer SR, and separation bubble SOR. Dissipations of the shear layer and the separation bubble can be negligible compared with those of shock waves, even though the dissipation may be strengthened by the vortex breakdown in the 2D recirculation zone.[24–26] The major cause is that the velocity gradient in a shock wave is much larger than those in the shear layer and the separation bubble [Eq. (3) implies that a larger velocity gradient induces a stronger dissipation]. See detailed analysis in Part 2 of the supplementary material. Therefore, the total dissipation Φ in V is primarily contributed by shock SB and RB and can be written as

$$\Phi = \int_V \phi \mathrm{d}V \approx \widehat{\phi}_{SB} L_{SB} + \widehat{\phi}_{RB} L_{RB}, \tag{4}$$

where L is the shock wave length and $\widehat{\phi}$ is the dissipation per unit length. We will show that both $\widehat{\phi}$ and L depend only on θ_s. With MVD theorem, a steady CFRLS can be determined by minimizing Φ among all possible θ_s.

By integrating Eq. (2) across the shock wave perpendicularly, $\widehat{\phi}$ can be written as

$$\widehat{\phi} = \int_\delta \phi \mathrm{d}n = \underbrace{-\int_\delta \rho \boldsymbol{u} \cdot \nabla\left(\frac{1}{2}|\boldsymbol{u}|^2\right)\mathrm{d}n}_{\mathcal{E}} + \underbrace{\int_\delta p\vartheta \mathrm{d}n}_{\mathcal{P}}, \tag{5}$$

where

$$\begin{aligned} \mathcal{E} &= \frac{1}{2}\left\{\rho_a (M_a c_a \sin\beta)^3 - \rho_b [M_b c_b \sin(\beta - \theta)]^3\right\}, \\ \mathcal{P} &\approx -\frac{1}{2}(p_a + p_b)[M_a c_a \sin\beta - M_b c_b \sin(\beta - \theta)], \end{aligned} \tag{6}$$

where δ is the thickness of the shock wave and n is the normal direction. $\mathcal{E}$ and $\mathcal{P}$ are the kinetic energy loss and the pressure work, respectively, implying that one portion of the kinetic energy loss is stored as the potential energy and the other is dissipated. c and β are the acoustic velocity and shock angle, respectively. Subscripts

"a" and "b" denote locations ahead of and behind a shock wave, respectively. Quantities on both sides of a shock wave satisfy

$$\left.\begin{array}{ll} M_b^2 = \mathcal{F}_M(M_a,\beta), & c_b/c_a = \mathcal{F}_c(M_a,\beta) \\ \rho_b/\rho_a = \mathcal{F}_\rho(M_a,\beta), & p_b/p_a = \mathcal{F}_p(M_a,\beta) \\ \mathcal{F}_\beta(M_a,\beta,\theta) = 0. & \end{array}\right\} \tag{7}$$

As shown in Fig. 1(a), for shock *SB* with shock angle β_s and deflection angle θ_s, "a" and "b" correspond to "0" and "1," respectively; for shock *SB* with β_r and $\theta_r = \alpha - \theta_s$, "a" and "b" correspond to "1" and "2," respectively. $\mathcal{F}_M$, $\mathcal{F}_c$, $\mathcal{F}_\rho$, $\mathcal{F}_p$, and $\mathcal{F}_\beta$ are the Rankine–Hugoniot relations (see Part 3 of the supplementary material). Applying Eq. (7) to shock *SB* and *RB*, the set of 10 governing equations contains 15 parameters, namely, $M_0, M_1, M_2, c_0, c_1, c_2, \rho_0, \rho_1, \rho_2, p_0, p_1, p_2, \beta_s, \beta_r$, and θ_s. For given free-stream conditions M_0, c_0, ρ_0 and p_0, the other 10 parameters can be determined with a certain θ_s. Using Eq. (5), we obtain $\widehat{\phi}_{SB}$ and $\widehat{\phi}_{RB}$ depending only on θ_s.

Then, we focus on the geometrical relationships of the flow system. The size (area) Ω_s of the separation bubble, approximated to a triangle,[14] is assumed to be constant for all possible θ_s with given M_0, α, and wall temperature T_w. This *a priori* assumption consists with that the mass of fluids in the separation bubble, $\Pi_s = \rho_s\Omega_s$, is proportional to the pressure rise $p_1(\theta_s)$ in the plateau region (p_{pla} is the steady p_1), since the bubble density $\rho_s = \gamma M_0^2 p_1/T_w$ is proportional to p_1. It provides a physical image that the stronger the p_1 is, the more fluids the separation bubble contains. Based on this assumption, L_{SB} and L_{RB} can be calculated by geometric relations (see details in Part 4 of the supplementary material),

$$\begin{aligned} \frac{L_{SB}}{\sqrt{\Omega_s}} &= \sqrt{\frac{2\sin\alpha}{\sin\theta_r\sin\theta_s}}\frac{\cos\theta_s\tan(\beta_r+\theta_s)-\sin\theta_s}{\cos\beta_s\tan(\beta_r+\theta_s)-\sin\beta_s}, \\ \frac{L_{RB}}{\sqrt{\Omega_s}} &= \sqrt{\frac{2\sin\alpha}{\sin\theta_r\sin\theta_s}}\frac{\cos\theta_s\tan\beta_s-\sin\theta_s}{\sin(\beta_r+\theta_s)-\cos(\beta_r+\theta_s)\tan\beta_s}. \end{aligned} \tag{8}$$

Note that β_s and β_r in Eq. (7) are both determined by θ_s and Ω_s remains constant. Therefore, L_{SB} and L_{RB} depend only on θ_s.

Combining Eqs. (4), (5), and (8), the total dissipation can be calculated. Figure 2(a) depicts the variation in $\Phi/\sqrt{\Omega_s}$ with all possible angles θ_s for different M_0 and α. Because a steady CRFLS configuration should maintain MVD, a steady θ_s fulfills

$$\frac{\partial\Phi}{\partial\theta_s} = 0, \quad \frac{\partial^2\Phi}{\partial\theta_s^2} > 0. \tag{9}$$

As shown in Fig. 2(a), there is only one minimal value of Φ for a combination of M_0 and α, indicating that only one steady state exists in a CRFLS, which is consistent with experimental observations. Figure 2(b) shows the variation in the theoretical steady θ_s for different M_0 and α. For a given α, θ_s is observed to decrease as M_0 increases. However, for a given M_0, three possible scenarios occur, i.e., (i) for relatively small M_0 [M_0 = 3, 6, 10 in Fig. 2(b)], θ_s increases with α, implying that a larger α can induce a higher p_{pla}; (ii) for relatively large M_0, θ_s increases first and then saturates (for M_0 = 14, $\theta_s \approx 5.7°$ when $\alpha > 35°$); and (iii) for sufficient large M_0, there is a critical α corresponding to a peak θ_s (for M_0 = 20, critical $\alpha \approx 26°$ and $\theta_s^{peak} \approx 4°$), over which θ_s will decrease as α increases. The first scenario has been observed,[26,27] while the second and third trends need further examination. It must be emphasized that the theoretical steady θ_s in Fig. 2(b) is mainly suitable for CRFLS ($\alpha^* > 2.5$), the occurrence of which also depends on *Re* and *C*.

TABLE I. Simulation setup.

Re (mm)	*Pr*	T_w/T_0	T_0 (K)	Flat plate/ramp lengths (mm)	Height (mm)
3000	0.7	1.5	108.1	80.0/112.7	40.0

To verify the present theory, 2D simulations are conducted with Open-CFD, source codes, and numerical methods, which have been widely validated.[28–31] Computational parameters (including the Prandtl number *Pr* and the free-stream temperature T_0) are presented in Table I. The first wall-normal grid height is fixed to 0.01 mm. For the Blasius boundary layer (attachment) with present *Re* and T_w, Δy^+ of the first grid is 0.98 at $x = -77$ mm and decreases to 0.43 at $x = 0$ mm. The resolution of the simulations is 3401 × 401 by clustering grid points near the wall. The grid convergence is shown in Fig. 3 that the two largest grid scale's C_f (3401 × 401 and 2801 × 281) collapse in all regions. The streamwise grid uniformly spaces with width 0.05 mm. We use $M_0 = 6.0$ at $\alpha = 16°, 20°, 24°$ ($\alpha^* = 4.43, 5.54, 6.65$) to study the ramp angle effect and $\alpha = 24°$ with $M_0 = 3.0, 4.5, 6.0$ ($\alpha^* = 9.61, 7.71, 6.65$) to study the Mach number effect.

Figure 4 shows the comparison of predicted θ_s, β_s, and β_r with our 2D simulations and previous numerical results.[1] Theoretical θ_s, β_s, and β_r (dashed lines) are drawn on present numerical density fields for more clear illustration and the previous numerical schlierens.[1] θ_s and β_s start at separation points, while β_r start at reattachment points. For each case, θ_s, β_s, and β_r match the

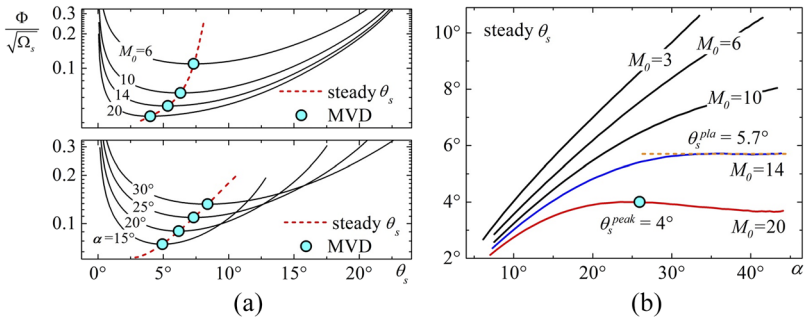

FIG. 2. (a) Variations in $\Phi/\sqrt{\Omega_s}$ with all possible θ_s. The cyan points—MVD, the red dashed lines—steady θ_s, upper panel—M_0 = 6 at α = 15°, 20°, 25°, 30°, and lower panel—α = 25° with M_0 = 6, 10, 14, 20. (b) Steady θ_s for different M_0 and α.

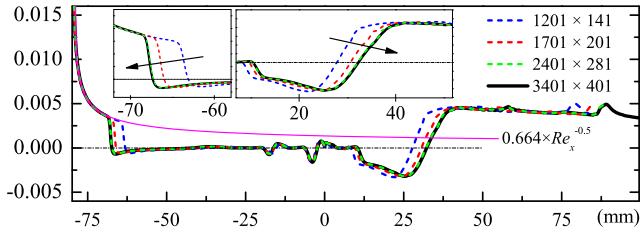

FIG. 3. Validation of grid convergence by C_f with four grid scale. The magenta line is the Blasius solution $C_f = 0.664Re_x^{-0.5}$. The main separation and reattachment have been zoomed-in in the inner graph.

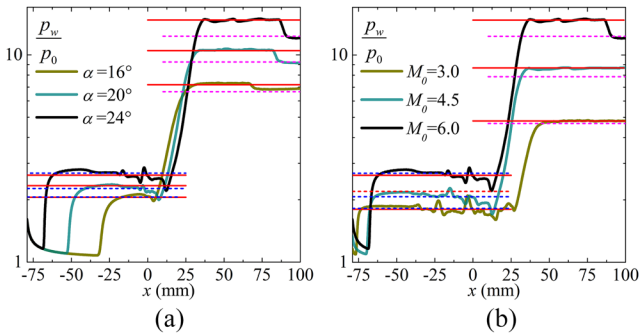

FIG. 5. Comparison of the predicted p_{pla} and p_{peak} with 2D simulations. Red solid lines—present theoretical predictions, blue dashed lines—FIT, and purple dashed lines—inviscid pressure rise. (a) $M_0 = 6.0$ at $\alpha = 16°$, 20°, 24°. (b) $\alpha = 24°$ with $M_0 = 3.0$, 4.5, 6.0.

inclinations of the shear layer, separation shock, and reattachment shock, respectively.

Figure 5 shows pressure distributions with large separation. It is seen that a large plateau region arises for each case, and a distinct peak region appears for $M_0 = 6.0$. Some fluctuations arise in both the plateau and peak regions due to the vortex breakdown in the recirculation zone (mainly exists in 2D cases[24–26]). In present theory, p_{pla} and p_{peak} correspond to p_1 and p_2 in Eq. (7) with steady θ_s, respectively. It is seen that both the p_{pla} prediction of FIT and present theory agree well with the simulations. FIT emphasizes that p_{pla} is "downstream-independent" and only depends on p_i and $C_{f,i}$ at the interaction origin. However, the location of interaction origin I should depend on the downstream conditions (such as the ramp angle α), i.e., the larger the α is, the closer the interaction origin is to the leading edge. Recent studies[14,32] also show that downstream influences should not be neglected. On the other hand, downstream information, related to the reattachment shock RB, could be transmitted upstream via the nearly incompressible separation bubble. The morphological adjustment of the separation bubble corresponds to the synergy of shock waves SB and RB, decreasing the total dissipation as much as possible. Therefore, the MVD theorem, as an integral method, can capture this global information, with which both p_{pla} and p_{peak} are predictable.

Figure 6 depicts the comparison of theoretical p_{peak} with previous studies, including experimental[27,33–35] and numerical[1,26,36–44] results. Some errors may be introduced by extracting data directly from quoted papers. As M_0 and α increase, p_{peak} increases rapidly and will be two orders of magnitude larger than p_0 for high M_0. It is seen that predictions of p_{peak}/p_0 agree well with most of the numerical and experimental results with M_0 varying from 3.0 to 14.1 and α varying from 15° to 38°. Additionally, as the maximum heat flux h_{peak} generated behind reattachment can be correlated with p_{peak} in terms of simple power-law relations,[17,42–46] the present theory can be used to estimate h_{peak} quantificationally.

In this work, MVD theorem is applied to CRFLS with effects of Mach number M_0 and ramp angle α. The steady deflection angle θ_s of outer-stream can be obtained by minimizing the dissipation. The predicted pressure plateau p_{pla} is consistent with present simulation results and FIT. With certain θ_s, the pressure peak p_{peak} is simultaneously obtained and agrees well with most of the numerical and experimental results for a wide range of M_0 and α. Besides, some

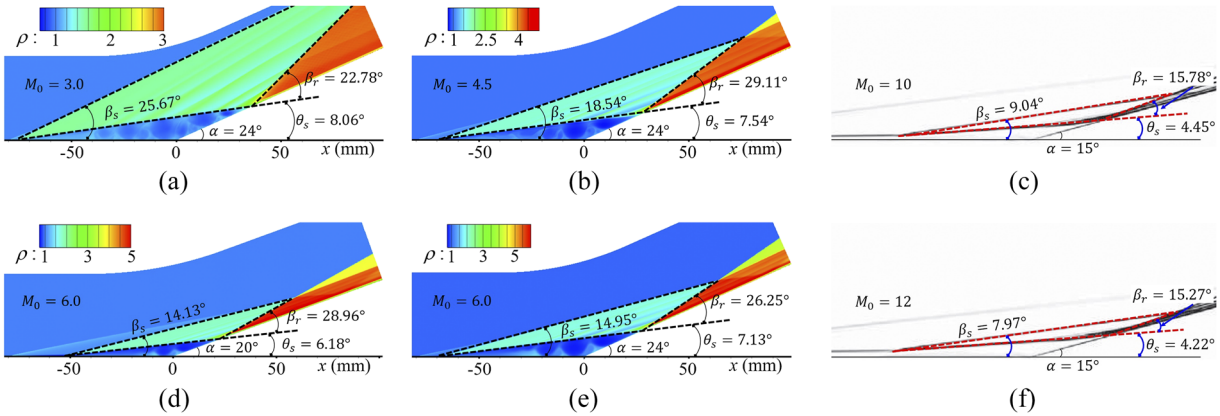

FIG. 4. Comparison of predicted θ_s, β_s, and β_r (dashed lines) with numerical results. [(a) and (b)] $M_0 = 3.0$ and $M_0 = 4.5$ at $\alpha = 24°$. [(d) and (e)] $\alpha = 20°$ and $\alpha = 24°$ with $M_0 = 6.0$ are present numerical density fields. (c) $M_0 = 10$ and (f) $M_0 = 12$ at $\alpha = 15°$ are numerical schlierens extracted from the work of Babinsky and Harvey[1] (pp. 318–319).

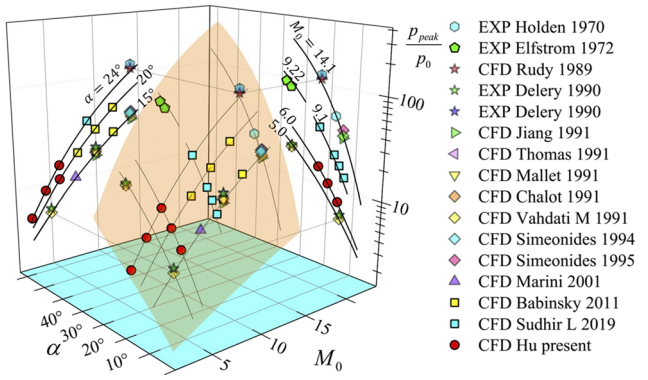

FIG. 6. Comparison of present theoretical p_{peak}/p_0 (the 3D orange surface) with numerical and experimental results (color points). These results and predictions (black lines) for different α and M_0 are also projected to the (M_0, p_{peak}/p_0)-plane and the (α, p_{peak}/p_0)-plane.

occurred deviations in the predictions may result from the effects of the Reynolds number Re or the wall temperature T_w, which will be investigated in future.

See the supplementary material for four parts.

We are grateful to Professor Xin-Liang Li and You-Sheng Zhang for their helpful discussions. This work was supported by the National Key R & D Program of China (Grant No. 2019YFA0405300).

DATA AVAILABILITY

The data that support the findings of this study are available from the corresponding author upon reasonable request.

REFERENCES

[1]H. Babinsky and J. K. Harvey, *Shock Wave-Boundary-Layer Interactions* (Cambridge University Press, 2011), Vol. 32.
[2]D. R. Chapman, D. M. Kuehn, and H. K. Larson, "Investigation of separated flows in supersonic and subsonic streams with emphasis on the effect of transition," NACA Technical Report 1356 pp. 421–460 (1958).
[3]G. Gadd, "A theoretical investigation of laminar separation in supersonic flow," J. Aeronaut. Sci. **24**, 759–771 (1957).
[4]L. Lees and B. L. Reeves, "Supersonic separated and reattaching laminar flows. I-General theory and application to adiabatic boundary-layershock-wave interactions," AIAA J. **2**, 1907–1920 (1964).
[5]K. Stewartson and P. Williams, "Self-induced separation," Proc. R. Soc. London, Ser. A **312**, 181–206 (1969).
[6]V. Y. Neiland, "Theory of laminar boundary layer separation in supersonic flow," Fluid Dyn. **4**, 33–35 (1969).
[7]K. Stewartson, "On laminar boundary layers near corners," Q. J. Mech. Appl. Math. **23**, 137–152 (1970).
[8]K. Stewartson and P. Williams, "On self-induced separation ii," Mathematika **20**, 98–108 (1973).
[9]R. Jenson, O. Burggraf, and D. Rizzetta, "Asymptotic solution for supersonic viscous flow past a compression corner," in *Proceedings of the Fourth International Conference on Numerical Methods in Fluid Dynamics* (Springer, 1975), pp. 218–224.
[10]D. Rizzetta, O. Burggraf, and R. Jenson, "Triple-deck solutions for viscous supersonic and hypersonic flow past corners," J. Fluid Mech. **89**, 535–552 (1978).
[11]J. Erdos and A. Pallone, "Shock-boundary layer interaction and flow separation," in *Proceedings of the 1962 Heat Transfer and Fluid Mechanics Institute* (Stanford University Press Stanford, CA, 1962), Vol. 15, pp. 239–254.
[12]O. Burggraf, "Asymptotic theory of separation and reattachment of a laminar boundary layer on a compression ramp," in *Flow Separation* (AGARD CP-168, 1975).
[13]P. Daniels, "Laminar boundary-layer reattachment in supersonic flow," J. Fluid Mech. **90**, 289–303 (1979).
[14]R. Giepman, F. Schrijer, and B. Van Oudheusden, "A parametric study of laminar and transitional oblique shock wave reflections," J. Fluid Mech. **844**, 187–215 (2018).
[15]B. Edney, "Anomalous heat transfer and pressure distributions on blunt bodies at hypersonic speeds in the presence of an impinging shock," Technical Report 115 (Flygtekniska Forsoksanstalten, Stockholm, Sweden, 1968).
[16]W. J. Guman, "On the plateau and peak pressure of regions of pure laminar and fully turbulent separation in two-dimensional supersonic flow," J. Aerosp. Sci. **26**, 56 (1959).
[17]B. Li, L. Bao, and B. Tong, "Theoretical modeling for the prediction of the location of peak heat flux for hypersonic compression ramp flow," Lixue Xuebao/Chin. J. Theor. Appl. Mech. **44**, 869–875 (2012).
[18]H. V. Helmholtz, "Zur theorie der stationären ströme in reibenden flüssigkeiten," Wiss. Abh. **1**, 223–230 (1868).
[19]Lord Rayleigh, "Lxv: On the motion of a viscous fluid," London, Edinburgh Dublin Philos. Mag. J. Sci. **26**, 776–786 (1913).
[20]J. Serrin, "Mathematical principles of classical fluid mechanics," in *Fluid Dynamics I/Strömungsmechanik I* (Springer, 1959), pp. 125–263.
[21]K. Ho, D. Yang, and J. Wu, "The extension of minimum energy dissipation theorem and the limitation of minimum entropy production principle in fluid flow," J. Eng. Thermophys. **9**, 10–12 (1988).
[22]J.-Z. Wu, H.-Y. Ma, and M.-D. Zhou, *Vorticity and Vortex Dynamics* (Springer Science & Business Media, 2007).
[23]Y.-C. Hu, Z.-G. Tang, Y.-G. Yang, W.-F. Zhou, and Z.-H. Qin, "Origin of hysteresis in shock wave reflection," preprint arXiv:2005.07905 (2020).
[24]F. T. Smith, "A reversed-flow singularity in interacting boundary layers," Proc. R. Soc. London, Ser. A **420**, 21–52 (1988).
[25]F. Smith and A. F. Khorrami, "The interactive breakdown in supersonic ramp flow," J. Fluid Mech. **224**, 197–215 (1991).
[26]S. L. Gai and A. Khraibut, "Hypersonic compression corner flow with large separated regions," J. Fluid Mech. **877**, 471–494 (2019).
[27]G. Elfstrom, "Turbulent hypersonic flow at a wedge-compression corner," J. Fluid Mech. **53**, 113–127 (1972).
[28]X. Li, D. Fu, Y. Ma, and X. Liang, "Direct numerical simulation of shock/turbulent boundary layer interaction in a supersonic compression ramp," Sci. China: Phys., Mech. Astron. **53**, 1651–1658 (2010).
[29]F. Tong, X. Li, Y. Duan, and C. Yu, "Direct numerical simulation of supersonic turbulent boundary layer subjected to a curved compression ramp," Phys. Fluids **29**, 125101 (2017).
[30]Z. Yan, X. Li, and C. Yu, "Scale locality of helicity cascade in physical space," Phys. Fluids **32**, 061705 (2020).
[31]Y.-C. Hu, W.-T. Bi, S.-Y. Li, and Z.-S. She, "β-distribution for Reynolds stress and turbulent heat flux in relaxation turbulent boundary layer of compression ramp," Sci. China: Phys., Mech. Astron. **60**, 124711 (2017).
[32]L. Xue, F. F. Schrijer, B. W. van Oudheusden, C. Wang, Z. Shi, and K. Cheng, "Theoretical study on regular reflection of shock wave–boundary layer interactions," J. Fluid Mech. **899**, A30 (2020).
[33]M. S. Holden and J. R. Moselle, "Theoretical and experimental studies of the shock wave-boundary layer interaction on compression surfaces in hypersonic flow," Aerospace Research Laboratories, USAF-OAR Report No. ARL-70-0002 (1968).
[34]J. Delery and M. Coet, "Experimental investigation of shock-wave boundary-layer interaction in hypersonic flows," in *Workshop on Hypersonic Flows for Reentry Problems* (Springer, 1990), Vol. 3, pp. 1–22.
[35]J. Delery and M.-C. Coet, "Experiments on shock-wave/boundary-layer interactions produced by two-dimensional ramps and three-dimensional obstacles," in *Hypersonic Flows for Reentry Problems* (Springer, 1991), pp. 97–128.

[36]D. Rudy, J. Thomas, A. Kumar, P. Gnoff, and S. Chakravarthy, "A validation study of four Navier-Stokes codes for high-speed flows," in *20th Fluid Dynamics, Plasma Dynamics and Lasers Conference* (AIAA, 1989), p. 1838.
[37]D. Jiang and B. Richards, "Hypersonic viscous flow over two-dimensional ramps," in *Hypersonic Flows for Reentry Problems* (Springer, 1991), pp. 228–243.
[38]J. L. Thomas, D. H. Rudy, A. Kumar, and B. Van Leer, "Grid-refinement study of hypersonic laminar flow over a 2-d ramp," in *Hypersonic Flows for Reentry Problems* (Springer, 1991), pp. 244–254.
[39]M. Vahdati, K. Morgan, and J. Peraire, "The application of an adaptive upwind unstructured grid solution algorithm to the simulation of compressible laminar viscous flows over compression corners," in *Hypersonic Flows for Reentry Problems* (Springer, 1991), pp. 201–211.
[40]M. Mallet, B. Mantel, J. Périaux, and B. Stoufflet, "Contribution to problem 3 using a Galerkin least square finite element method," in *Hypersonic Flows for Reentry Problems* (Springer, 1991), pp. 255–267.
[41]F. Chalot, T. Hughes, Z. Johan, and F. Shakib, "Application of the Galerkin/least-squares formulation to the analysis of hypersonic flows: I. Flow over a two-dimensional ramp," in *Hypersonic Flows for Reentry Problems* (Springer, 1991), pp. 181–200.
[42]G. Simeonides, W. Haase, and M. Manna, "Experimental, analytical, and computational methods applied to hypersonic compression ramp flows," AIAA J. **32**, 301–310 (1994).
[43]G. Simeonides and W. Haase, "Experimental and computational investigations of hypersonic flow about compression ramps," J. Fluid Mech. **283**, 17–42 (1995).
[44]M. Marini, "Analysis of hypersonic compression ramp laminar flows under sharp leading edge conditions," Aerosp. Sci. Technol. **5**, 257–271 (2001).
[45]M. Holden, "A study of flow separation in regions of shock wave-boundary layer interaction in hypersonic flow," in *11th Fluid and PlasmaDynamics Conference* (AIAA, 1978), p. 1169.
[46]G. M. Currao, R. Choudhury, S. L. Gai, A. J. Neely, and D. R. Buttsworth, "Hypersonic transitional shock-wave–boundary-layer interaction on a flat plate," AIAA J. **58**, 814–829 (2020).